Analysis of Yagi–Uda-Type Antennas

GARY A. THIELE, MEMBER, IEEE

Abstract—A method of analyzing Yagi–Uda-type antennas is presented. Since the Yagi–Uda array is a fairly well-known antenna, it is used as an example to demonstrate the application and accuracy of the method. However, the method of solution is not limited to a planar array, such as the Yagi, but can be applied to arrays of nonplanar linear elements. The approach taken in analyzing Yagi–Uda antennas is based on rigorous equations for the electric field radiated by the elements in the array. All interactions are taken into account. Calculated results are presented for the Yagi–Uda array that show excellent agreement with experimental results reported in the literature. In addition, the dependence of the far-field patterns on the phase velocity is shown. It is also demonstrated that the phase velocity is generally nonuniform along the array.

Introduction

IN 1927 and 1928, respectively, Uda and Yagi published their papers on what today is known as the Yagi–Uda antenna [1], [2]. Much is known about the Yagi–Uda array, but this has been due mostly to experimental data rather than a method of theoretical investigation. There are, however, some exceptions. One is a paper published by Wilkinshaw in 1946 which applied only to short (4 directors) Yagi–Uda antennas [3]. A theoretical and experimental paper by Green gives design data for several practical Yagi–Uda arrays [4]. His method was the classical one in which the Yagi–Uda array is viewed as a special kind of center-driven dipole array in which all but the actual exciter element are short-circuited at the terminals. Currents are induced in the parasitic elements via the mutual impedances with the exciter, and radiation occurs as from a set of discrete sources. Green has analyzed arrays with up to ten elements using this method with good results.

Ehrenspeck and Poehler have published an interesting experimental paper in which they describe a method for obtaining maximum gain from a Yagi–Uda array [5]. Their method is based on achieving the proper phase velocity along the array, but the resulting effect of the phase velocity on the far-field patterns is not shown. They imply equal phase delay from director to director. However, calculations made with the technique described in this paper indicate that the phase progression along the array is nonuniform.

Serracchioli and Levis theoretically investigated the phase velocity of long endfire uniform dipole arrays [6]. Their curves provide information relating element radius, length, and spacing to the phase velocity. This information is useful in the initial selection of these parameters when using the technique presented here. The longer the Yagi under consideration, the more applicable are their curves.

Mailloux has developed a method for approximately analyzing the behavior of finite Yagi arrays [7]. His method essentially consists of truncating a semi-infinite array and then calculating the reflection coefficient at the end of the array. He presents results for a 20-element reflectorless array. More recently King has applied his three-term theory to a uniform Yagi–Uda array [8].

The following discussion describes a method of theoretically studying the complex current distributions on all the elements of a Yagi–Uda array, the phase velocity and the corresponding radiation patterns. The technique is based on rigorous equations for the electric field radiated by the elements in the array. All interactions are taken into account. There appears to be no restriction imposed by the method itself on how few or how many elements may be in the array. However, the size of the digital computer employed to do the computations will place an upper limit on the number of elements that may be considered. Typically, it has been found that the storage capacity of the IBM 7094 is sufficient to enable 27 elements to be simultaneously included in the calculations.

Excellent agreement between calculated results obtained by this method and experimental results reported in the literature were obtained. In addition, these results enable one to show clearly the dependence of the far-field patterns on the phase velocity along the array.

Formulation of the Problem

The approach taken in formulating this method of solving the Yagi–Uda-type antenna problem is based on an integral equation for the electric field of the array. The point-matching technique is then used to satisfy the integral equation at discrete points on the axis of each element rather than attempting to satisfy this equation everywhere on the surface of every element [9]–[13]. Thus a system of linear algebraic equations is generated in terms of the complex coefficients in the Fourier series expansion of the currents on the elements. Inversion of the matrix yields the value of these coefficients from which the current distributions, phase velocity, and far-field patterns may readily be obtained. Experience has shown that if one chooses a sufficient number of points at which to match boundary conditions, then one can obtain solutions to problems, such as this one, heretofore not easily solvable.

In the case of linear elements, such as those in Fig. 1, it has been found that an efficient representation for the current on element p is

$$I_p(z) = \sum_{n=1}^{N} I_{n_p} \cos (2n - 1) \frac{\pi z}{L}. \quad (1)$$

Manuscript received May 8, 1968; revised September 11, 1968.
The author is with the ElectroScience Laboratory, Department of Electrical Engineering, Ohio State University, Columbus, Ohio 43212.

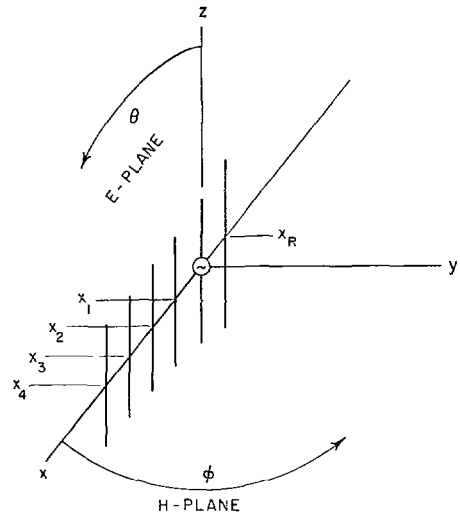

Fig. 1. Coordinate system used to analyze Yagi–Uda array.

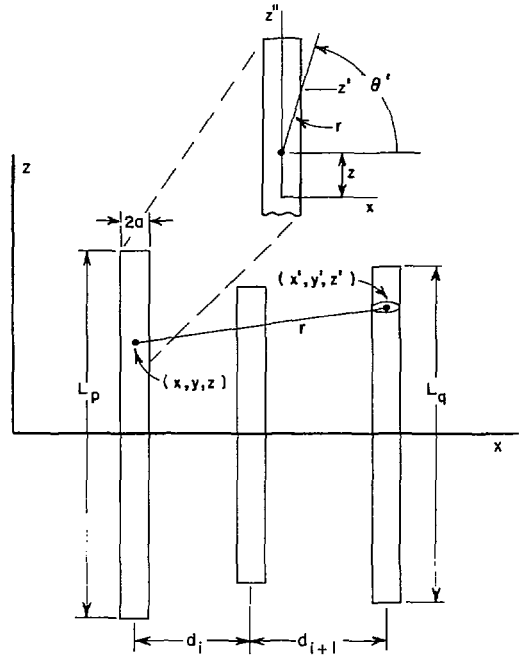

Fig. 2. Diagram showing distance from a matching point (observation point) on pth element to source region on qth element. Insert shows relationship between z' and θ' when observation point and source region are on the same element.

This series of odd-ordered even modes is chosen such that the current goes to zero at the ends of element p. This is a suitable approximation for elements whose diameter is small in terms of the wavelength. Also, this series has been used by the author in treating the thin linear antenna or dipole [13].

From the vector potential may be derived an integral expression for the electric field radiated by the array. This integral expression is

$$E_z(x,y,z) = \frac{\lambda\sqrt{\mu/\epsilon}}{8\pi^2 j}\sum_{p=1}^{D+2}\sum_{n=1}^{N} I_{n_p}\int_{-L_p/2}^{L_p/2} G(x,y,z|x',y',z') \cdot \cos\,(2n-1)\frac{\pi z'}{L_p}\,dz' \quad (2)$$

where

$$G(x,y,z|x',y',z') = \frac{\exp\,[-jkr]}{r^5}\,[(1+jkr)(2r^2-3a^2) + k^2a^2r^2] \quad (3)$$

and

$$r = \sqrt{(x'-x)^2+(y'-y)^2+a^2+(z'-z)^2} \quad (4)$$

as shown in Fig. 2.

It has been found that z' is an efficient variable of integration when the current on wire p is observed at a matching point on element q, $p \neq q$. However, when $p = q$, it is more efficient to use θ' as the variable of integration since the integrand varies rapidly when $z' \approx z$. Details of this change of variables may be found in [9]. For either variable of integration, the integral in (2) is carried out numerically.

System of Linear Equations

Considerable insight into the point-matching technique, when applied to a problem as complex as the Yagi–Uda array, can be obtained by looking at the system of linear equations and the resulting matrix representation. For the moment, let us consider an array composed of D directors, a reflector, and a driven element. Let us have N modes on each element, but let each element be of different length. Using (2), the first part of the system of equations is then of the form

$$\sum_{p=1}^{D+2}\sum_{n=1}^{N} C_{m,n_p}I_{n_p} = 0, \quad m = 1, 2, \cdots, N \times D. \quad (5)$$

These equations are generated by requiring that tangential E be zero at N points on each director. That is to say, tangential E is zero at a total of $N \times D$ points on the directors. The matching points on any one director are illustrated in Fig. 3.

The next N equations are similar to the previous $N \times D$ equations since tangential E vanishes at N points on the reflector element, as shown in Fig. 3. Thus

$$\sum_{p=1}^{D+2}\sum_{n=1}^{N} C_{m,n_p}I_{n_p} = 0,$$

$$m = (N \times D) + 1, \cdots, N \times (D+1). \quad (6)$$

The last N equations are generated by using the boundary condition on the driven element, as shown in Fig. 4. That is,

$$\sum_{p=1}^{D+2}\sum_{n=1}^{N} C_{m,n_p}I_{n_p} = 0,$$

$$m = N \times (D+1) + 1, \cdots, N \times (D+2) - 1 \quad (7)$$

and

$$\sum_{n=1}^{N} I_{n_e} = 1, \quad e = D+2, \quad m = N \times (D+2). \quad (8)$$

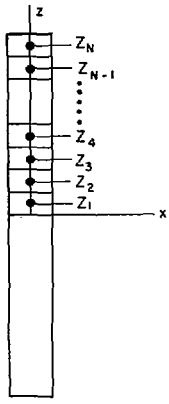

Fig. 3. Parasitic element with N matching points along its axis.

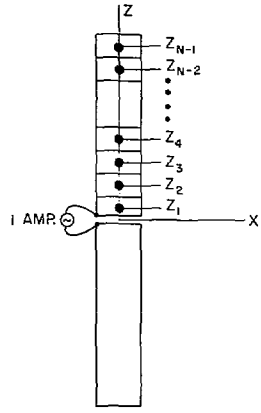

Fig. 4. Driven element with $N - 1$ matching points along its axis.

On the driven element the tangential E boundary condition is only enforced at $N - 1$ points even though there are N modes. The Nth equation on the exciter arises from the constraint on the terminal current value [13].

Computer Program[1]

A discussion of the computer program is, perhaps, facilitated by considering a simple example. Consider an array composed of a director, a reflector, and a driven element. Further, assume only two modes on each element. Thus the complete system for this example would be similar to

$$\begin{bmatrix} C_{11} & C_{12} & C_{13} & C_{14} & C_{15} & C_{16} \\ C_{21} & C_{22} & C_{23} & C_{24} & C_{25} & C_{26} \\ C_{31} & C_{32} & C_{33} & C_{34} & C_{35} & C_{36} \\ C_{41} & C_{42} & C_{43} & C_{44} & C_{45} & C_{46} \\ C_{51} & C_{52} & C_{53} & C_{54} & C_{55} & C_{56} \\ 0 & 0 & 0 & 0 & 1 & 1 \end{bmatrix} \cdot \begin{bmatrix} I_1 \\ I_2 \\ I_3 \\ I_4 \\ I_5 \\ I_6 \end{bmatrix} = \begin{bmatrix} 0 \\ 0 \\ 0 \\ 0 \\ 0 \\ 1 \end{bmatrix}.$$

The physical interpretation of the matrix elements is as follows: at point z_1 on element 1 (the director), C_{11} is the "field" generated by mode 1, and C_{12} is the field generated at the same point by mode 2. C_{21} is the field generated by mode 1 at point z_2 on the director, and C_{22} is that of mode 2. In a similar manner we can interpret C_{33}, C_{34}, C_{43}, and C_{44}.

If we write the above matrix in a submatrix representation,

$$\begin{bmatrix} S_{11} & S_{12} & S_{13} \\ S_{21} & S_{22} & S_{23} \\ S_{31} & S_{32} & S_{33} \end{bmatrix} \cdot \begin{bmatrix} I_1 \\ I_2 \\ I_3 \\ I_4 \\ I_5 \\ I_6 \end{bmatrix} = \begin{bmatrix} 0 \\ 0 \\ 0 \\ 0 \\ 0 \\ 1 \end{bmatrix}$$

[1] Requests for additional information on the computer program may be addressed as follows: Director, ElectroScience Laboratory, Ohio State University, 1320 Kinnear Road, Columbus, Ohio 43212.

then it is apparent that, regardless of the number of submatrices, those on the main diagonal of submatrices will represent the field generated by the current on the element at which the tangential E boundary condition is being enforced. Hence if there are D identical directors, the first D submatrices on the main diagonal will all be identical. This fact is utilized to shorten the running time of the program but is no restriction on the method itself which could be used on tapered or modulated structures.

For elements off the main diagonal of submatrices the following reasoning applies. The quantity C_{35} represents the field at point 1 on element 2 (the reflector) due to the first mode (mode 5) on the driven element (element 3). A similar interpretation applies to C_{36}, C_{45}, and C_{46}. Thus submatrices S_{qr}, $q \neq r$, represent the interaction between elements q and r. If all the directors are of the same length, then $S_{qr} = S_{rq}$ for director submatrices. Further, for uniform director spacing there will be several inter-director spacings or distances that will be the same. Consider the 4-director Yagi in Fig. 1. The distance between directors 1 and 3 is the same as that between 2 and 4, for instance. Hence $S_{13} = S_{24}$, assuming the directors are of the same length.

Thus we see that it may not be necessary to calculate all the submatrices individually, and, consequently, a significant savings in computer time is realized when working with long and complex problems that require large amounts of numerical integration. The program developed for this problem utilizes the above mentioned techniques. However, the program is not restricted to uniform director spacing. It simply takes advantage of geometrical symmetries that may exist.

Once the entire matrix has been calculated, it is easily solved by standard methods for the coefficients I_{np} in the Fourier series representation of the currents on the various elements. Using these currents, the far-field patterns may be obtained in a straightforward manner.

Far-Field Patterns

The far-field pattern of a single element of the Yagi antenna in Fig. 1 is given by

$$E_\theta(\theta) = \frac{j\omega\mu}{4\pi r_0} \exp\left[-jkr_0\right] \sin\theta \int_{-L/2}^{L/2} I(z') \cdot \exp\left[jkz \cos\theta\right] dz'. \quad (9)$$

Since the current is expressed as a Fourier series, we obtain

$$E_\theta(\theta) = \frac{-jL\sqrt{\mu/\epsilon}}{\pi r_0} \exp\left[-jkr_0\right] \sin\theta \cdot \sum_{n=1}^{N} (-1)^n \frac{(2n-1)I_n \cos(\pi L' \cos\theta)}{(2n-1)^2 - (2L' \cos\theta)^2} \quad (10)$$

where $L' = L/\lambda$. Since

$$r_0 \approx r - (x \sin\theta \cos\phi + y \sin\theta \sin\phi + z \cos\theta) \quad (11)$$

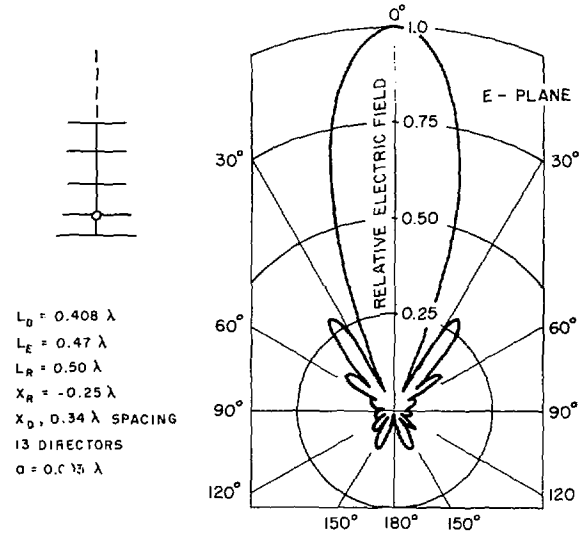

Fig. 5. E-plane pattern of 15-element Yagi–Uda array.

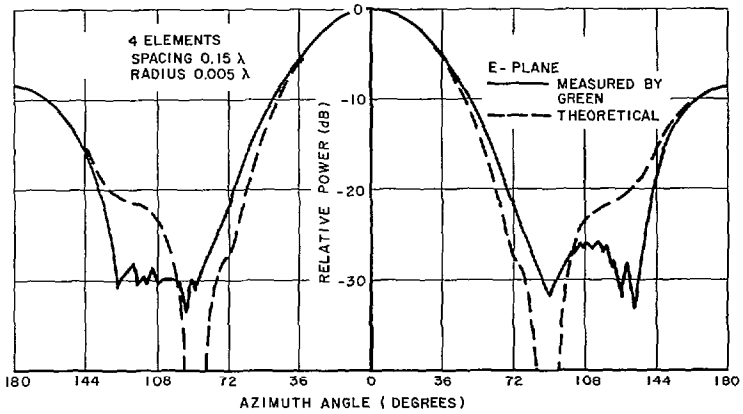

Fig. 6. E-plane pattern of 4-element Yagi–Uda array.

we can define a pattern factor

$$F(\theta,\phi) = L_p \sin\theta \exp\left[+jk(x_p \sin\theta\cos\phi + y_p \sin\theta\sin\phi + z_p\cos\theta)\right] \sum_{n=1}^{N} (-1)^n \cdot \frac{(2n-1)I_{n_p}\cos(\pi L'\cos\theta)}{(2n-1)^2 - (2L'\cos\theta)^2}. \quad (12)$$

Thus if we have W elements each with N modes, we may write for the total pattern factor $F_T(\theta,\phi)$,

$$F_T(\theta,\phi) = \sin\theta \sum_{p=1}^{W} L_p \exp\left[+jk(x_p \sin\theta\cos\phi + y_p \sin\theta\sin\phi + z_p\cos\theta)\right] \sum_{n=1}^{N} (-1)^n \cdot \frac{(2n-1)I_{n_p}\cos(\pi L'\cos\theta)}{(2n-1)^2 - (2L'\cos\theta)^2}, \quad W = D + 2. \quad (13)$$

If the number of modes on each element is not the same, then the above expression is necessarily more complicated. In practice, it has been found desirable to retain more modes on the driven element than are required for the parasitic elements. Hence the computer program actually allows for K modes on the former and N modes on the latter.

Results

Excellent results were obtained with the point-matching method applied to the Yagi–Uda antenna problem. The patterns calculated by this method agree quite well with experimental patterns published in the literature [4], [14]. For example, Fig. 5 shows a calculated E-plane pattern for a 15-element Yagi–Uda array. The pattern agrees so well with an experimental one published by Fishenden and Wiblin [14] that there is no reason to attempt to distinguish between them in the figure. In this and subsequent figures L_D, L_E, and L_R are, respectively, the director length, exciter length, and reflector length. As implied by Fig. 1, X_R is the x coordinate of the reflector, and X_D indicates the uniform director spacing. Fig. 6 shows an experimental power plot of a 4-element array published by Green [4]. Good agreement is seen to exist between the experimental pattern and the theoretical

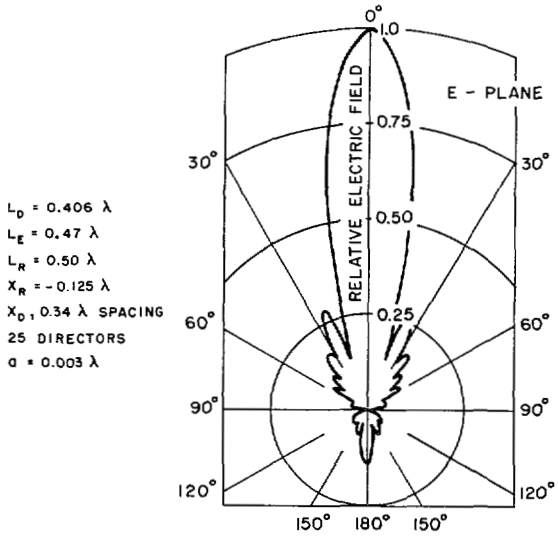

Fig. 7. *E*-plane pattern of 27-element Yagi–Uda array.

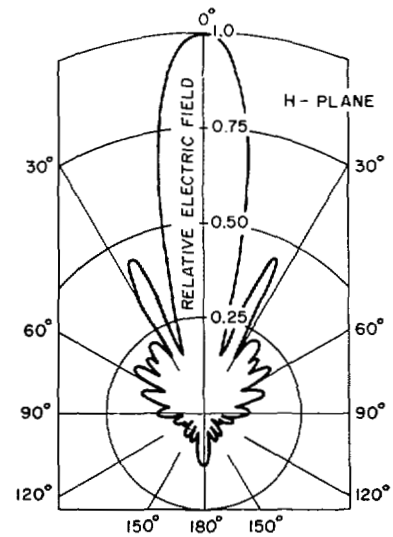

Fig. 8. *H*-plane pattern for array o Fig. 7.

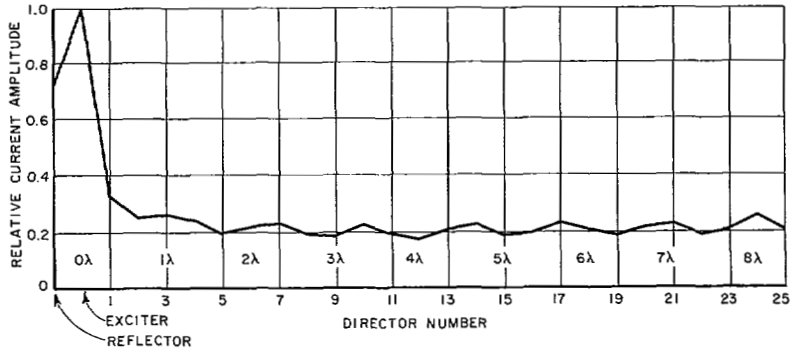

Fig. 9. Relative current amplitudes for array of Fig. 7.

one obtained with the point-matching method. In fact, the front-to-back ratio is precisely the same.

Figs. 7 and 8 show calculated *E*-plane and *H*-plane patterns, respectively, for a 27-element array. This was the largest number of elements that could be handled conveniently by the computer program on the IBM 7094. With a computer of larger memory more elements could be accommodated. It is interesting to note that the *E*-plane pattern of this 27-element array is similar to a measured pattern also published by Fishenden and Wiblin for a 32-element array with a slightly longer director length of 0.408λ. All other parameters were the same. Fig. 9 shows a plot of the current amplitudes on all of the 27 elements. This plot clearly shows that the director currents are not equal nor are they smoothly tapered in the forward direction. It will be shown later that the progressive phasing of the currents is also not uniform, even for uniform director spacing.

There are two principle ways in which the far-field pattern of a Yagi–Uda array may be "tuned" or adjusted for a particular frequency. One way is to vary the director spacing while holding the element length and reflector spacing constant. The second method is to vary the director length while holding all other parameters fixed. Either one of these methods will have a considerable effect on the far-field patterns. On the other hand, the usual effects of altering the reflector spacing or length are mostly to change the level of the back lobe and to control the impedance of the array. Further, changing the length of the driven element will have a negligible effect on the pattern. Of course, as one would expect, altering the exciter length will change the input impedance of the array. A method of calculating the array input impedance is under consideration.

All of the aforementioned changes that affect the far-field pattern do so because they alter the phase velocity along the array. Hence it is reasonable to use this as a design criteria rather than simply observing the change in far-field patterns due to a change in director length and/or spacing, etc.

The Hansen–Woodyard condition for an endfire array states that for increased directivity in the forward direction it is necessary to have a total phase delay of almost 180 degrees along the array. That is to say, the phase velocity needs to be slower than the corresponding free-space phase velocity. The Hansen–Woodyard condition assumes equal amplitudes in the array elements. However, as seen in Fig. 9, this is not the situation for a Yagi–Uda array. Nevertheless, it is possible to draw a vector diagram which will show when the array has been prop-

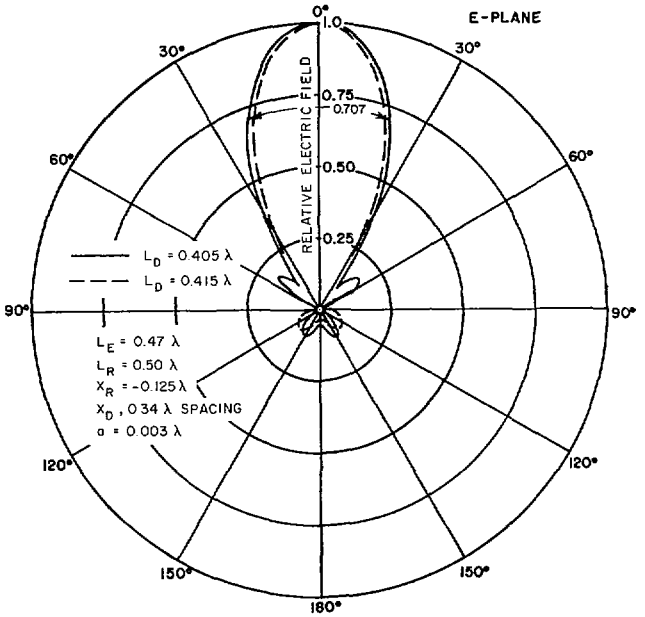

Fig. 10. *E*-plane patterns of two 8-element arrays.

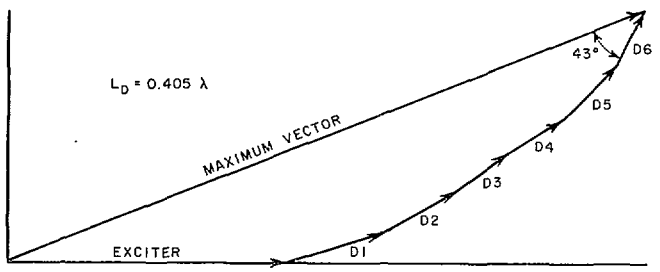

Fig. 11. Phase velocity diagram for 8-element array with L_D = 0.405λ.

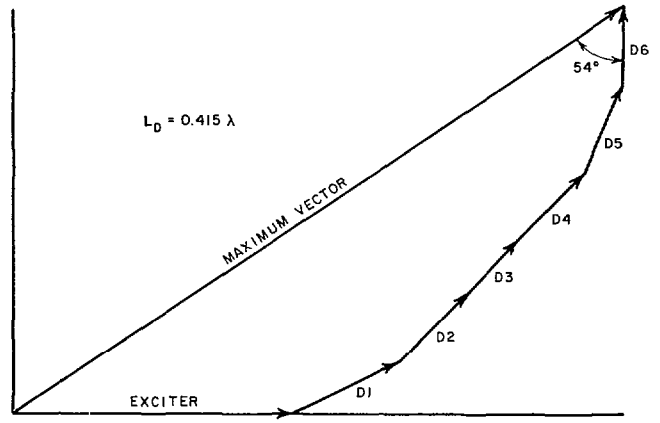

Fig. 12. Phase velocity diagram for 8-element array with L_D = 0.415λ.

erly adjusted for increased directivity in the forward direction. The vector diagram will, of course, take into account the unequal amplitudes in the various elements. Furthermore, the diagram will afford much greater insight into the behavior of the array. Such diagrams have been published by Ehrenspeck and Poehler [5]. However, they indicate equal phase delay from director to director. Calculations with the point-matching method show that this is not the case; a result which is not illogical when one considers the complexity of the finite array and the fact that the current amplitudes are unequal.

Fig. 10 shows two patterns of an 8-element array. We observe that an increase in the director length has caused a narrowing of the main beam without an increase in the side lobes. Thus we might expect that the phase velocity on the $L_D = 0.415\lambda$ array is somewhat slower than that for $L_D = 0.405\lambda$. Inspection of Figs. 11 and 12 shows this to be true. Fig. 11 shows a plot of the current amplitudes on the exciter and directors. The change in direction from one vector to the next is determined by taking the difference between the calculated phase progression and that which would exist if the phase velocity were that of free space. Hence if the phase velocity were that of free space, all the vectors would lie along the horizontal axis. Further, if the phase velocity were uniform, the change in direction from one vector to the next would be the same for any two adjacent vectors (assuming uniform director spacing). Examination of Fig. 12, for instance, shows that such is not the case. Thus we may conclude that the phase velocity is generally nonuniform. In principle, this finding is in agreement with Damon's results for endfire dipole arrays [15].

As additional phase delay is achieved, the tip of the last vector ($D6$ in this situation) moves away from the horizontal axis and toward the vertical axis. The maximum vector is defined to be that vector from the origin to the tip of the component vector farthest from the origin. Thus we see in Figs. 10–12 that by increasing the director lengths we have slightly increased the directivity in the forward direction because the phase velocity has been decreased.

It should be mentioned that although the point-matching method permits one to obtain more accurate results than are generally obtainable by other methods, one should not infer that the director lengths given here are meaningful in practice to more than two decimal places. What is meaningful, however, is the change in phase velocity due to a given change in director lengths, as discussed in the following paragraphs.

Figs. 13 and 14 show the vector diagrams for successively longer director lengths. We note that in Fig. 14 the maximum vector is not to the tip of the last vector $D6$. When this situation occurs, it indicates that the phase delay is excessive, and, consequently, that the far-field pattern will start to deteriorate. To see that this is indeed the case, we refer to Fig. 15. Here we see the pattern for the case $L_D = 0.4275\lambda$. Also indicated are the back and side lobe levels for several other cases. Comparing Fig. 15 with Fig. 10, we immediately see that the main beam in the former is significantly less than in the latter. This is consistent with what the vector diagrams indicate.

In Figs. 13–15 we see that as the maximum vector approaches the point where it no longer extends to the tip of $D6$, but to $D5$ instead, the lobes in the pattern start to come up quickly, especially the back lobe. At the same time the beamwidth is decreased only a very

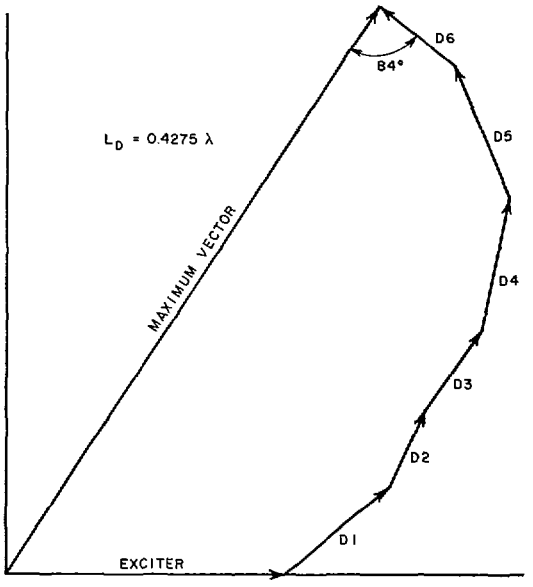

Fig. 13. Phase velocity diagram for 8-element array with L_D = 0.4275λ.

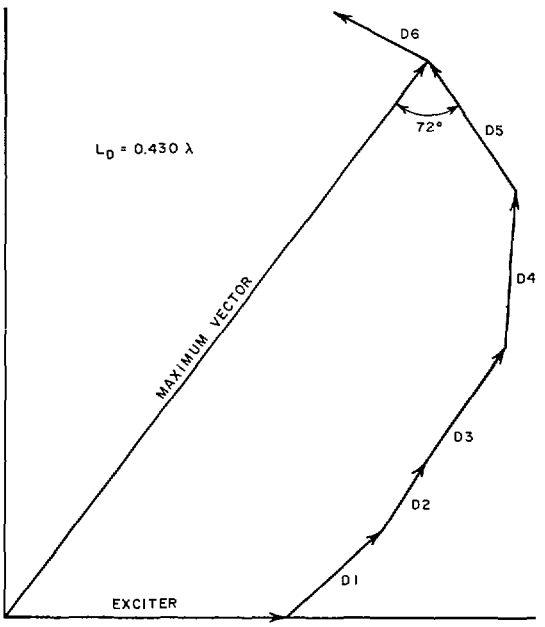

Fig. 14. Phase velocity diagram for 8-element array with L_D = 0.430λ.

slight amount. Specifically, for L_D = 0.4250λ, it is about 2 degrees wider than the pattern for L_D = 0.4275λ, about 2 degrees narrower for L_D = 0.4300λ, and about 4 degrees narrower than indicated in Fig. 15 for L_D = 0.4350λ.

Consequently, it would appear that in the design of a Yagi–Uda array one should strive to keep the phase velocity at or above that which would produce a vector diagram similar to Fig. 13. From another viewpoint we can interpret the slower phase velocity as giving rise to a backward surface wave which is evidenced most prominently in an increasing back lobe. In fact, the computer printout shows an increasing current amplitude on the reflector element in such cases.

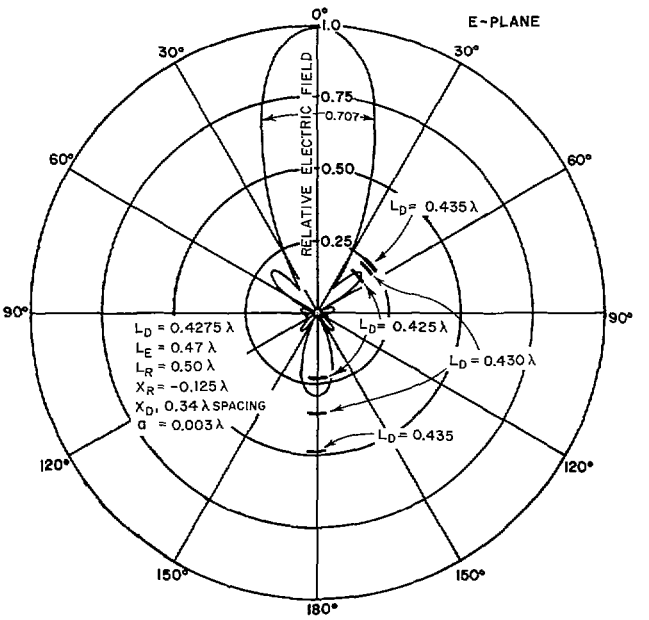

Fig. 15. *E*-plane pattern of optimum 8-element array with side lobe levels indicated for several other versions of array.

Conclusion

A method of analyzing the Yagi–Uda array by using the point-matching or linear equation technique has been presented. The method is general in that it may be applied to nonplanar arrays with an arbitrary number of elements having arbitrary length and with arbitrary spacing between them. While there is essentially no minimum number of elements that may be considered, the maximum number appears to be limited only by the size of the digital computer available. For instance, 27 elements were accommodated by the program on the IBM 7094 by using three modes on each of the parasitic elements and seven on the driven element. In addition, this method of analysis permits one to obtain accurate information not only about the far-field patterns, but also on the current distributions and phase velocity as well. One could also investigate the scattering behavior of such arrays by removing the generator and exciting the antenna with a plane wave.

This method need not be limited to the one reflector, *D*-director-type of Yagi–Uda array depicted in Fig. 1, but it may easily be extended to other antenna configurations using linear elements or elements that may be subdivided into linear elements such as in a vee configuration. Consequently, the various elements would not need to be parallel with one another as they are in the Yagi–Uda array. In such cases it would be necessary to consider the contribution to the tangential electric field at a matching point by the radial component of the electric field in addition to the z component given here. Further, current distributions that are not symmetrical about the center of the elements may be handled by the inclusion of the modes $\sin 2n\pi z/L_p$ in the current expansion for $I_p(z)$.

Finally, the use of a computerized approach in the investigation and design of Yagi-Uda-type antennas presents several distinct advantages over an experimental approach. Among these are the obvious savings in the expenditure of time and money and also the possibility of obtaining antennas optimized with respect to directivity, side lobe levels, bandwidth, or any weighted combination of these.

Acknowledgment

The author wishes to acknowledge the support of the Ohio State University Numerical Computation Laboratory, which provided the computer time for the Yagi-Uda antenna calculations. The author also wishes to thank Profs. C. H. Walter and J. H. Richmond for their helpful comments.

References

[1] S. Uda, "Wireless beam of short electric waves," *J. IEE* (Japan), pp. 273–282, March 1926, and pp. 1209–1219, November 1927.
[2] H. Yagi, "Beam transmission of ultra short waves," *Proc. IRE*, vol. 16, pp. 715–741, June 1928.
[3] W. Wilkinshaw, "Theoretical treatment of short Yagi aerials," *Proc. IEE* (London), pt. 3, vol. 93, p. 598, 1946.
[4] H. E. Green, "Design data for short and medium length Yagi-Uda arrays," *Elec. Engrg. Trans. Inst. Engrs.* (Australia), pp. 1–8, March 1966.
[5] H. W. Ehrenspeck and H. Poehler, "A new method for obtaining maximum gain from Yagi antennas," *IRE Trans. Antennas and Propagation*, vol. AP-7, pp. 379–386, October 1959.
[6] F. Serracchioli and C. A. Levis, "The calculated phase velocity of long end-fire uniform dipole arrays," *IRE Trans. Antennas and Propagation*, vol. AP-7, pp. S424–S434, December 1959.
[7] R. J. Mailloux, "The long Yagi-Uda array," *IEEE Trans. Antennas and Propagation*, vol. AP-14, pp. 128–137, March 1966.
[8] R. W. P. King, "The linear antenna—eighty years of progress," *Proc. IEEE*, vol. 55, pp. 2–16, January 1967.
[9] J. H. Richmond, "Digital computer solutions of the rigorous equations for scattering problems," *Proc. IEEE*, vol. 53, pp. 796–804, August 1965.
[10] R. F. Harrington, "Matrix methods for field problems," *Proc. IEEE*, vol. 55, pp. 136–149, February 1967.
[11] Y. S. Yeh and K. K. Mei, "Theory of conical equiangular-spiral antennas. Part I—Numerical technique," *IEEE Trans. Antennas and Propagation*, vol. AP-15, pp. 634–639, September 1967.
[12] V. R. Arens, C. T. Elfving, U. R. Emlory, and D. L. Johnstone, "Integral equation formulation of a log periodic antenna," *1967 IEEE G-AP Internat'l Symp. Dig.* (Ann Arbor, Mich., October 17–19), pp. 55–63.
[13] G. A. Thiele, "Calculation of the current distribution on a thin linear antenna," *IEEE Trans. Antennas and Propagation (Communications)*, vol. AP-14, pp. 648–649, September 1966.
[14] R. M. Fishenden and E. R. Wiblin, "Design of Yagi aerials," *Proc. IEE* (London), pt. 3, vol. 96, pp. 5–13, January 1949.
[15] E. K. Damon, "The near fields of long end-fire dipole arrays," *IRE Trans. Antennas and Propagation*, vol. AP-10, pp. 511–523, September 1962.

Radiation from Elliptic Current Rings

G. N. TSANDOULAS, MEMBER, IEEE

Abstract—**A solution is given for the radiation fields due to a current sustained in an elliptic ring of arbitrary dimensions. Although the case examined is that of a constant current, the study can serve as the basic formalism by which other distributions may be treated. The derived results apply directly to the elliptical capacitive antenna and the elliptical annular slot.**

I. Introduction

EVER SINCE 1944 when Foster [1] obtained a solution for the far fields of a circular current loop, a number of investigators have examined the circular shape extensively [2]–[4]. Whereas the circular loop has received considerable attention, other geometrical shapes are less understood. Understandably, the circle is of great practical importance. Its utilization in a wide variety of applications more or less obviated the need for investigation of other figures. Nevertheless, the elliptical cylindrical antenna has received some attention [5]. It was finally recognized that the circle and ellipse are connected by a linear transformation, a fact used to advantage by Lo and Hsuan [6] in systematizing and simplifying calculations involving elliptical arrays.

Interest in the elliptical current ring stems from two considerations. First, the radiation pattern is a function of the azimuthal coordinate φ as well as the polar θ. As a result, different directive properties are exhibited as the φ plane is scanned, a fact that might be desirable in some applications. Second, there are two degrees of freedom available to the designer (the lengths of the two principal axes or, equivalently, the interfocal distance and the eccentricity) rather than one, as is the case of the circle.

The analysis covers as extensions the elliptic capacitor antenna consisting of two elliptic plates of small separation and the elliptic annular slot, just as the analysis of the circular ring leads to the solution of the circular capacitive antenna and the circular annular slot. Formal interchange of electric and magnetic fields is, of course, necessary in both cases.

Manuscript received May 13, 1968; revised August 9, 1968.
The author is with the M.I.T. Lincoln Laboratory, Lexington, Mass. 02173 (operated with support from the Advanced Research Projects Agency).